

# Paying Attention to Multiscale Feature Maps in Multimodal Image Matching

Aviad Moreshet      Yosi Keller  
 Bar-Ilan University, Israel  
 {aviad10m, yosi.keller}@gmail.com

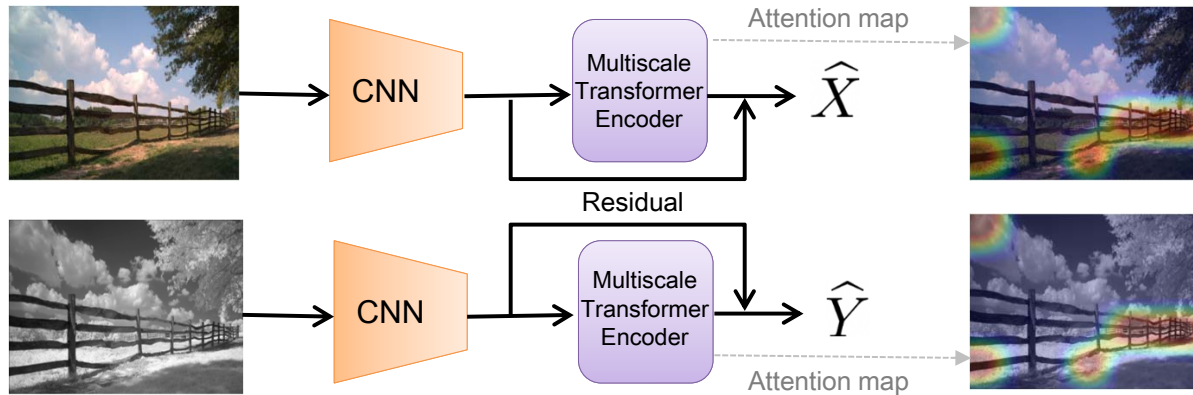


Figure 1: The proposed attention-based approach. A Siamese backbone CNN computes the feature maps of the input multimodal image patches, that are passed through a Spatial Pyramid Pooling (SPP) layer [17]. A Transformer encoder aggregates the multiscale image embeddings. A residual connection bypasses the Encoder to facilitate end-to-end training. The attention heatmaps visualize the modality-invariant visual cues emphasized by the attention scheme.

## Abstract

We propose an attention-based approach for multimodal image patch matching using a Transformer encoder attending to the feature maps of a multiscale Siamese CNN. Our encoder is shown to efficiently aggregate multiscale image embeddings while emphasizing task-specific appearance-invariant image cues. We also introduce an attention-residual architecture, using a residual connection bypassing the encoder. This additional learning signal facilitates end-to-end training from scratch. Our approach is experimentally shown to achieve new state-of-the-art accuracy on both multimodal and single modality benchmarks, illustrating its general applicability. To the best of our knowledge, this is the first successful implementation of the Transformer encoder architecture to the multimodal image patch matching task.

## 1. Introduction

Image patch matching is a fundamental task in computer vision aiming to determine the correspondence between two image patches. Multimodal patch matching focuses on

matching patches originating from different sources, such as visible RGB and near-infrared (NIR). Such patches are inherently more difficult to match due to the non-linear and unknown variations in pixel intensities, varying lighting conditions and colors. In particular, multimodal images are the manifestations of different physical attributes of the depicted objects, and the acquisition devices. There are a gamut of multimodal patch matching applications, such as fusing information in medical imaging devices [35] and multi-sensor images alignment [19].

Pioneering work [11, 18, 1] extended classical local image descriptors such as SIFT [24] and SURF [7] to multimodal matching, attempting to derive appearance-invariant feature descriptors. The resulting descriptors were matched using the Euclidean distance, but showed limited results, being unable to capture high-level structural information. Recently, deep learning models were shown to be the most effective [5, 4, 14, 6, 38], allowing improved performance across multiple modalities. Contemporary state-of-the-art (SOTA) approaches are based on training a Siamese CNN [21], either by directly outputting pairwise patch matching probabilities [41, 40, 14], or by outputting the patches feature descriptors and encoding their similarity in a latent

space [34, 26, 36], an approach denoted as descriptor learning.

Different losses were used to optimize the networks. Cross-Entropy Loss can be used [40, 4, 14] to classify the image patches as in a binary same/not-same classification task. Contrastive [34, 6] and Triplet Losses [26] were used along with Euclidean distance to learn descriptors encoding latent space similarity. Due to the high ratio of negative pairs, most of which being easy negatives barely contributing to the loss, hard negative mining schemes have become prevalent in recent studies [5, 26, 6, 20], sometimes combined with hard positive mining [34, 4, 38].

We propose a novel approach for attention-based multimodal patch matching. The gist of our approach, shown in Fig. 1, is to apply attention using a Transformer encoder to aggregate multiscale image embeddings into a unified image descriptor. The descriptors are learnt for both modalities by a weight-sharing Siamese network, that simultaneously learns the joint informative cues in both patch modalities. In particular, as depicted in the attention heatmaps visualized in Figs. 1 and 3, the modality-invariant informative visual cues correspond to the largest attention activations, computed by the encoder. Other image locations that are less task-informative show weak attention activations. To apply the Transformer Encoder, we formulate the matching task as a sequence-to-one problem, where the inputs are multimodal feature maps flattened into sequences and the outputs are adaptively aggregated embeddings. The spatial layout information of the image embeddings is induced by positional encoding. Due to the lack of pre-trained CNN backbones for multimodal patch matching, the backbone CNN has to be trained from scratch, starting from randomly initialized weights. This, in turn, prevents the encoder from learning meaningful sequence summarizations at the beginning of the training process, hindering the overall learning. To mitigate this issue, we propose to add a residual connection to the network bypassing the Transformer encoder, ultimately allowing end-to-end training of the proposed architecture from scratch. Our approach is experimentally shown to achieve new SOTA multimodality matching performance on multiple contemporary datasets.

In conclusion, our contribution is threefold:

1. A novel attention-based approach for multimodal image patch matching by aggregating multiscale Siamese CNN feature maps, using the Transformer encoder. To the best of our knowledge, this is the first application of the Transformer encoder architecture to the multimodal image patch matching task.
2. We propose a residual connection bypassing the encoder to enable end-to-end training from scratch, a crucial requirement in the absence of pre-trained weights for the task.

3. Our approach is experimentally shown to achieve new SOTA results on contemporary multimodal image patch matching benchmarks VIS-NIR [3] and En *et al.* [4, 14]. We also achieve new SOTA performance on the single modality UBC Benchmark [9], showing the generalizability of our approach.

## 2. Related work

### 2.1. CNN-based approaches for image matching

Deep learning techniques became the staple of computer vision, and were applied to multi-modality matching, showing SOTA performance. Jahrer *et al.* [21] introduced a Siamese CNN network for metric learning of feature descriptors, outperforming classic handcrafted descriptors such as SIFT [24]. Han *et al.* [40] added a metric learning network on top of a Siamese CNN, achieving SOTA results while also decreasing the size of the learned descriptors. Zagoruyko and Komodakis [41] explored multiple Siamese-based CNN architectures. The first is a 2-Channel architecture where the patches are concatenated channel-wise and are fed to a single CNN. The second is a Pseudo-Siamese CNN network with non-shared weights, and the last is a central-surround architecture, in which two Siamese CNNs are jointly trained with different input resolutions to better capture multi-resolution information. All methods presented promising results on the reported benchmarks. Aguilera *et al.* [3] extended those architectures to the multimodal case, outperforming previous approaches. Balntas *et al.* suggested a weight-sharing triplet CNN termed PN-Net [5], using image triplets consisting of two matching patches alongside a non-matching one. A new curated loss was also introduced to replace hard negative mining, by penalizing small  $L_2$  distances between non-matching pairs and large  $L_2$  distances between matching pair, forcing the network to always perform backpropagation using the hardest non-matching sample of each triplet. Aguilera *et al.* proposed a cross-spectral extension to the previous work, a weight-sharing quadruple network called Q-Net [4], utilizing two pairs of cross-spectral patches. The loss was extended to the quadruple case, mining both hard positive and hard negative samples at the same time. L2-Net [36] proposed by Tian *et al.* addressed an inherent problem in patch matching where the number of negative samples is orders of magnitude larger than positive samples, by picking  $n^2 - n$  hard negative samples per batch with a minimum distance to the  $n$  positive batch pairs. Mishchuk *et al.* proposed the HardNet [26] extension to L2-Net [36] using a curated hard negatives sampling scheme, ensuring that the distance of the selected negative sample is minimal. Both approaches achieved SOTA performance in unimodal benchmarks. Wang *et al.* introduced a novel Exponential Loss function [38] forcing the network to learn more from both

positive and negative hard samples than from easy ones. The scheme combines hard negative and positive mining inspired by Mishchuk *et al.* [26] and Simo *et al.* [34], respectively. Irshad *et al.* followed this line with the Twin-Net [20] approach, by proposing to mine twin negatives along with a dedicated Quad Loss, designed for single modality patches. In twin negatives mining, the first negative is mined as in Mishchuk *et al.* [26], and its closest negative is picked as the second negative. The Quad Loss then forces the descriptors of the chosen positive and anchor to be closer than the twin negatives descriptors, resulting in descriptors with a greater discriminatory power.

En *et al.* proposed an approach to utilize both joint and modality-specific information within the image patches, by combining Siamese and Pseudo Siamese CNNs in a unified architecture dubbed TS-Net [14]. Ben-Baruch and Keller [6] built a similar hybrid framework fusing Siamese and Pseudo Siamese CNNs features through fully connected layers. Contrary to TS-Net [14], their approach calculated  $L_2$ -optimized patch descriptors essential for patch matching, and optimized the network using multiple auxiliary losses. These extensions have proven vital and resulted in SOTA performance on various multimodal benchmarks, introducing significant improvement. Quan *et al.* proposed the AFD-Net framework [30] consisting of three sub-networks, the first, aggregates multi-level feature differences, the second extracts domain-invariant features from image patch pairs, while the final one infers matching labels. This approach computes a patch similarity score, rather than image embeddings. Thus,  $\mathcal{O}(n^2)$  forward passes of the network are required for matching two images containing  $n$  image patches each, in contrast to  $\mathcal{O}(n)$  forward passes in a metric learning approach such as ours.

## 2.2. Transformer-based approaches in computer vision

The Transformer architecture was introduced by Vaswani *et al.* [37] as a novel formulation of attention-based approaches, allowing the encoding of sequences without RNN layers such as LSTM and GRU. Transformers were first applied in Natural Language Processing tasks [12], and then proved successful in a gamut of computer vision schemes [8, 10, 13, 27, 32]. Transformers, in contrast to convolution networks, are capable of aggregating long-range interactions between a sequence of input vectors. In computer vision, we can formulate the outputs of a backbone CNN as a sequence as in [10, 32, 13] and encode them using a Transformer encoder that aggregates spatial interactions (attention weights) between the activation map entries. Task-informative entries are numerically emphasized, compared to the non-informative ones. The Transformer architecture is composed of stacked layers of self-attention encoders and decoders attending the encoder out-

puts using a set of vectors denoted as queries. Using self-attention, the encoder produces a weighted average over the values of its inputs, such that the weights are produced dynamically using a similarity function between the inputs. Transformers-based Encoders and Decoders utilize multiple stacked Multi-Head Attention and Feed Forward layers. In contrast to the sequentially-structured RNNs, the relative position and sequential order of the sequence elements are induced by positional encodings, that are added to the Attention embeddings. In this work, we propose to combine a Siamese CNN for feature extraction with self-attention implemented by a Transformer encoder, adaptively weighing the feature maps according to their task-specific contribution, resulting in richer feature descriptors, leading to better multimodal matching capabilities.

## 3. Multiscale attention-based multimodal patch matching

We propose a novel attention-based approach for multimodal image patch matching by encoding Siamese CNN multiscale feature maps using the Transformer encoder architecture. We also introduce a residual connection bypassing the encoder, that is crucial for end-to-end training. We model the task as a sequence-to-one problem, where the inputs are multiscale feature maps of patches transformed into sequences, and the output is a learned feature descriptor. An overview of the proposed scheme is shown in Fig. 1.

Let  $\{\mathbf{X}, \mathbf{Y}\} \in \mathbb{R}^{H \times W \times C}$  be a pair of multimodal image patches. We first compute the corresponding activation maps  $\{\tilde{\mathbf{X}}, \tilde{\mathbf{Y}}\} \in \mathbb{R}^{\tilde{H} \times \tilde{W} \times \tilde{C}}$  using the backbone Siamese CNN. A Spatial Pyramid Pooling (SPP) layer [17] is applied to  $\{\tilde{\mathbf{X}}, \tilde{\mathbf{Y}}\}$ , to compute the  $K$  multiscale activation maps  $\{\tilde{\mathbf{X}}_k, \tilde{\mathbf{Y}}_k\} \in \mathbb{R}^{\tilde{H}_k \times \tilde{W}_k \times \tilde{C}}$ , as detailed in Section 3.1. Each of  $\{\tilde{\mathbf{X}}_k, \tilde{\mathbf{Y}}_k\}$  is flattened into sequences and aggregated into a single vector by the Transformer encoder, as in Section 3.2. A fully connected layer finally maps the output representations into  $\{\hat{\mathbf{X}}, \hat{\mathbf{Y}}\} \in \mathbb{R}^{128}$ . We also propose a novel residual connection described in Section 3.3 that bypasses the Transformer encoder and allows end-to-end training. The network is trained end-to-end using the Triplet Loss [33] and a symmetric formulation of the Hard-Net approach [26] detailed in Section 3.4.

### 3.1. Backbone CNN

For every pair of multimodal image patches  $\{\mathbf{X}, \mathbf{Y}\}$ , we apply a Siamese CNN to extract the feature maps  $\{\tilde{\mathbf{X}}, \tilde{\mathbf{Y}}\}$ . The CNN architecture is described in Table 1. We use the same backbones as previous works, to experimentally exemplify the efficiency of the proposed attention-based scheme in Section 4. Each convolutional layer is followed by Batch Normalization and ReLU activation. We use an SPP layer [17] consisting of a four-level pyramid

pooling, transforming the CNN feature maps into  $K$  multiscale feature maps  $\{\tilde{\mathbf{X}}_k, \tilde{\mathbf{Y}}_k\} \in \mathbb{R}^{\tilde{H}_k \times \tilde{W}_k \times \tilde{C}}$  such that  $\{\tilde{\mathbf{H}}_k, \tilde{\mathbf{W}}_k\} \in \{8, 4, 2, 1\}$ .

Layer	Output	Kernel	Stride	Pad	Dilation
Conv0	$64 \times 64 \times 32$	$3 \times 3$	1	1	1
Conv1	$64 \times 64 \times 32$	$3 \times 3$	1	1	1
Conv2	$31 \times 31 \times 64$	$3 \times 3$	2	1	2
Conv3	$31 \times 31 \times 64$	$3 \times 3$	1	1	1
Conv4	$29 \times 29 \times 128$	$3 \times 3$	1	1	2
Conv5	$29 \times 29 \times 128$	$3 \times 3$	1	1	1
Conv6	$29 \times 29 \times 128$	$3 \times 3$	1	1	1
Conv7	$29 \times 29 \times 128$	$3 \times 3$	1	1	1

Table 1: The Siamese backbone CNN architecture.

### 3.2. Multiscale Transformer encoder

The proposed weight-sharing Transformer encoder aggregates the  $K$  multiscale outputs of the backbone CNN and SPP layer, and is illustrated in Fig. 2. The encoder has two layers, each consisting of two multi-head attention blocks. Given  $K$  multiscale feature maps  $\{\tilde{\mathbf{X}}_k, \tilde{\mathbf{Y}}_k\}$ , each map is spatially flattened into a sequence of size  $\tilde{H}_k * \tilde{W}_k * \tilde{C}$ . We prepend a learnable embedding to each sequence whose corresponding output is the aggregated result, same as in [12]. In order to induce spatial information to the permutation-invariant Transformer encoder, we learn separable 2D positional encodings. The encodings are learned separately for the  $X$  and  $Y$  axes to reduce the number of learned parameters, and are denoted as  $\mathbf{E}_X \in \mathbb{R}^{\tilde{H}_k \times \frac{\tilde{C}}{2}}$  and  $\mathbf{E}_Y \in \mathbb{R}^{\tilde{W}_k \times \frac{\tilde{C}}{2}}$  respectively. The final 2D positional encoding  $\mathbf{E}_{i,j} \in \mathbb{R}^{\tilde{C}}$  is given by:

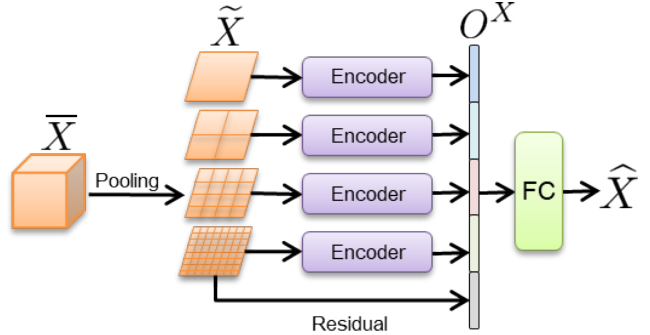
$$\mathbf{E}_{i,j} = \begin{bmatrix} \mathbf{E}_X^j \\ \mathbf{E}_Y^i \end{bmatrix}, [i, j] \in [1 \dots \tilde{H}_k, 1 \dots \tilde{W}_k] \quad (1)$$

The positional encodings are then spatially flattened into a sequence of size  $\tilde{H}_k * \tilde{W}_k * \tilde{C}$  and fed along with the feature map sequences to the encoder. The Transformer encoder is applied to produce  $K$  aggregations of the flattened embeddings  $\{\tilde{\mathbf{X}}_k, \tilde{\mathbf{Y}}_k\}$ , denoted  $\{\mathbf{O}_k^X, \mathbf{O}_k^Y\}$ .  $\{\mathbf{O}_k^X\}$  and  $\{\mathbf{O}_k^Y\}$  are separately concatenated into two vectors of dimension  $\mathbb{R}^{4\tilde{C}}$ , alongside the residual connections embedding  $\{\tilde{\mathbf{X}}_8, \tilde{\mathbf{Y}}_8\} \in \mathbb{R}^{8 \times 8 \times \tilde{C}}$ , as discussed in Section 3.3. Each of the two concatenated embedding is then passed through an FC layer and  $L_2$  normalized.

### 3.3. The residual connection

It is common to apply attention layers to pre-trained backbone CNNs that are kept frozen during the training process, allowing the Transformer encoder to train based on

Figure 2: The proposed multiscale Transformer encoder architecture.  $\bar{\mathbf{X}}$  is a feature map computed by the backbone CNN, and pooled into four multiscale feature maps  $\tilde{\mathbf{X}}_k$  by a SPP layer [17]. The Transformer encoder aggregates the pooled maps  $\tilde{\mathbf{X}}_k$ , and the aggregations  $\mathbf{O}_k^X \in \mathbb{R}^{128}$  are concatenated alongside the residual connection.



meaningful feature representations computed by the backbone. In contrast, in multimodal matching the backbone has to be trained end-to-end from scratch, due to the absence of pre-trained weights for the task. Thus, at the beginning of the training, until the CNN learns to extract useful feature maps, the encoder does not manage to learn meaningful sequence aggregations either, hindering the overall learning. We propose to tackle this problem by passing the last pooled feature map straight to the output layer using a residual connection, circumventing the encoder during its initialization phases, adding a vital learning signal which ultimately allows end-to-end training from scratch. As exemplified in Table 5, our architecture cannot be trained from scratch without this residual connection. Finally, the concatenated output is mapped by a fully connected layer  $FC$  producing feature descriptors for each pair of patches, denoted as  $\{\hat{\mathbf{X}}, \hat{\mathbf{Y}}\} \in \mathbb{R}^{128}$ .

### 3.4. Symmetric triplet loss

The proposed network is trained by applying the Triplet Loss [33] to the outputs  $\{\hat{\mathbf{X}}, \hat{\mathbf{Y}}\}$ :

$$L_t(a_i, p_j, n_k) = \sum_{n,j,k}^N \max(0, m + d(a_i, p_j) - d(a_i, n_k)) \quad (2)$$

where  $a_i, p_j$  and  $n_k$  are triplets of positive, anchor and negative samples,  $m$  is a margin, and  $d$  is the Euclidean distance. We used  $m = 1$  which is a common choice for the margin that also worked well in previous works. We also experimented using other values, but the performance was not improved. We chose  $d$  as the Euclidean distance function to be able to utilize efficient large-scale K-nearest-neighbors search schemes for descriptors matching in  $L_2$  spaces [15]. As the hard negative  $n_k$  is dynamically chosen within each



batch following the HardNet approach [26], we utilize the symmetry between  $a_i, p_j$  and train the network using a symmetrized formulation of Eq. 2 as follows:

$$L_t^s(a_i, p_j, n_k) = L_t(a_i, p_j, n_k) + L_t(p_j, a_i, n_k) \quad (3)$$

For each positive pair of patches  $a_i, p_i$  originated from different modalities, we first pick the hard negative as the negative sample in the batch closest to  $a_i$  and compute  $L_t(a_i, p_j, n_k)$ . The process is repeated mutandis mutatis by choosing the negative sample closest to  $p_i$  and computing  $L_t(p_j, a_i, n_k)$ .

## 4. Experimental Results

We evaluate the proposed scheme using multiple contemporary multimodal patch matching datasets. We use their publicly available setups that provide a *deterministic* generation of matching and non-matching train and validation patches. This allows a repeatable experimental setup that is shared and utilized by us and the SOTA schemes we compare against. We also demonstrate the generalizability of our proposal by evaluating it on the UBC Benchmark [9], a single modality, general benchmark for patch matching that was used in previous works. We measure our performance using the false positive rate at 95% recall (FPR95), where a smaller FPR95 score is better.

### 4.1. Datasets

The VIS-NIR Benchmark [3] is a cross-spectral image patch matching benchmark consisting of over 1.6 million RGB and Near-Infrared (NIR) patch pairs of size  $64 \times 64$ . The benchmark was collected by Aguilera *et al.* [3, 4] from the public VIS-NIR scene dataset. Half of the patches are matching pairs and half are non-matching pairs chosen at random. A public domain code<sup>1</sup> by Aguilera *et al.* allows to deterministically recreate the training and test sets, and was used by all schemes we compare against. The En *et al.* Benchmark [14] consists of three different multimodal datasets sampled on a uniform grid layout, with a corresponding public domain code<sup>2</sup>. VeDAI [31], consisting of vehicles in aerial imagery, CUHK [39], consisting of faces and face sketch pairs, and VIS-NIR [3]. Following En *et al.* setup [14], 70% of the data is used for training, 10% for validation and 20% for testing.

UBC Benchmark [9], also known as Brown Benchmark, is a single modality dataset consisting of image pairs sampled from 3D reconstructions. The benchmark consists of three subsets: Liberty, Notredame, and Yosemite, consisting of 450K, 468k, and 634K patches respectively. Patches

were extracted using Difference of Gaussian or Harris detector. Half of the patches, with the same 3D point, are matching pairs, and the rest are non-matching pairs. Following [9, 36, 41, 26] we iteratively train on one subset and test on 100k pairs of the other subsets.

### 4.2. Training

We use PyTorch [28] with three NVIDIA GeForce GTX 1080 Ti GPUs. Networks are randomly initialized from a normal distribution and optimized using Adam [23] with an initial learning rate of 0.1. A warmup learning rate scheduler [16] was used for eight epochs, and then replaced with a scheduler reducing the learning rate by a factor 10 every plateau of three epochs. The architecture was trained for 70 epochs using 48 size batches. Patches were mean-centered and normalized, and basic augmentations of horizontal flips and rotations were applied. The architecture is trained with random negatives until there is no loss decrease for three epochs. We then start mining hard negative samples using Mishchuk *et al.* technique [26].

### 4.3. VIS-NIR Benchmark

To demonstrate the effectiveness of our approach on the multimodal image patch matching task, we compare it with 14 state-of-the-art methods, using the same setup as Aguilera *et al.* [3] and [14, 4, 6]. The Country category is split into 80% and 20% for training and validation, respectively. The rest of the categories are used for testing. The results are shown in Table 2. We compare our proposal to both handcrafted descriptors [24, 25, 2] and state-of-the-art deep learning methods. We quote the results reported by [38, 6] on this benchmark.

For the handcrafted descriptors [24, 25, 2] we used their publicly available code. As in previous works, such approaches are outperformed by learning-based methods due to their inability to capture high-level semantic information. PN-Net [5], L2-Net [36], HardNet [26] and Exp-TLoss [38] are general-purpose, single modality schemes that were applied to the VIS-NIR Benchmark by Wang *et al.* [38]. These approaches that are based on a Siamese CNN architecture, same as the proposed scheme, generalized well to the multimodal case. Aguilera *et al.*'s three proposals [3] of vanilla Siamese CNN, Pseudo Siamese CNN, 2-Channel CNN, as well as SCFDM [29] and D-Hybrid-CL [6] were specifically designed for multimodal image patch matching and were tested on the VIS-NIR Benchmark. Our proposed scheme outperforms all previous approaches, achieving a new SOTA on this benchmark. In particular, it surpasses the previous SOTA Exp-TLoss [38] by 43% and D-Hybrid-CL [6] by 18%. Both methods are based on *the same* backbone CNN and SPP layer. Thus, we attribute the improved performance to the proposed attention-based inference, as opposed to previous schemes [38, 6] that are lim-

<sup>1</sup>VIS-NIR benchmark public setup code: <https://github.com/ngunsu/lcsis>

<sup>2</sup>En *et al.* benchmark setup code: <https://github.com/ensv/TS-Net>

Method	Field	Forest	Indoor	Mountain	Old building	Street	Urban	Water	Mean
Handcrafted descriptor methods									
SIFT [24]	39.44	11.39	10.13	28.63	19.69	31.14	10.85	40.33	23.95
MI-SIFT [25]	34.01	22.75	12.77	22.05	15.99	25.24	17.44	32.33	24.42
LGHD [2]	16.52	3.78	7.91	10.66	7.91	6.55	7.21	12.76	9.16
Learning-based methods									
Siamese [3]	15.79	10.76	11.6	11.15	5.27	7.51	4.6	10.21	9.61
Pseudo Siamese [3]	17.01	9.82	11.17	11.86	6.75	8.25	5.65	12.04	10.32
2-Channel [3]	9.96	0.12	4.4	8.89	2.3	2.18	1.58	6.4	4.47
PN-Net [5]	20.09	3.27	6.36	11.53	5.19	5.62	3.31	10.72	8.26
Q-Net [4]	17.01	2.70	6.16	9.61	4.61	3.99	2.83	8.44	6.86
TS-Net [14]	25.45	31.44	33.96	21.46	22.82	21.09	21.9	21.02	24.89
SCFDM [29]	7.91	0.87	3.93	5.07	2.27	2.22	0.85	4.75	3.48
L2-Net [36]	16.77	0.76	2.07	5.98	1.89	2.83	<b>0.62</b>	11.11	5.25
HardNet [26]	10.89	0.22	1.87	3.09	1.32	1.30	1.19	2.54	2.80
Exp-TLoss [38]	5.55	0.24	2.30	1.51	1.45	2.15	1.44	1.95	2.07
D-Hybrid-CL [6]	<b>4.4</b>	0.20	2.48	1.50	1.19	1.93	0.78	<b>1.56</b>	1.7
<b>Ours</b>	4.22	<b>0.13</b>	<b>1.48</b>	<b>1.03</b>	<b>1.06</b>	<b>1.03</b>	0.9	1.9	<b>1.44</b>

Table 2: Patch matching results evaluated on the VIS-NIR Benchmark [3]. Score is given in terms of FPR95.

ited to the multiscale SPP-based inference without the spatial attention-based aggregation.

#### 4.4. En *et al.* Benchmark

We compare our approach on this multimodal, multi-dataset benchmark following En *et al.* [14] publicly available setup<sup>3</sup> with ten state-of-the-art methods, both handcrafted [24, 25, 2] and learning-based [3, 4, 14, 6]. The results are reported at Table 3. We quote the results of previous schemes reported by [14, 6] on this benchmark.

On the VeDAI dataset, both 2-Channel [3], Hybrid [6] variants and our approach achieve zero error. On CUHK, our approach achieves the same performance as Hybrid-CE [6]. CUHK is a dataset composed of pairs of faces along with their face sketches. In this case, where the features are relatively limited and spatially close to each other, it seems that self-attention over the feature maps might not capture additional information. Nonetheless, we establish a new SOTA on the VIS-NIR dataset, improving it by 93%.

#### 4.5. UBC Benchmark

To illustrate the generalizability of our approach, we compare it with 11 state-of-the-art methods using the popular single modality UBC Benchmark [9], and the publicly available setup and evaluation code<sup>4</sup>, that was used by all the schemes we compare against. The results are presented in Table 4. We quote the previous results reported on this benchmark by [38, 20].

<sup>3</sup>En *et al.* benchmark setup code: <https://github.com/ensv/TS-Net>

<sup>4</sup>UBC benchmark setup and evaluation code: <https://github.com/osdf/datasets/tree/master/patchdata>

Method	VeDAI	CUHK	VIS-NIR
Handcrafted descriptor methods			
SIFT[24]	42.74	5.87	32.53
MI-SIFT [25]	11.33	7.34	27.71
LGHD[2]	1.31	0.65	10.76
Learning-based methods			
Siamese[3]	0.84	3.38	13.17
Pseudo Siamese[3]	1.37	3.7	15.6
2-Channel[3]	<b>0</b>	0.39	11.32
Q-Net[4]	0.78	0.9	22.5
TS-Net[14]	0.45	2.77	11.86
Hybrid-CE [6]	<b>0</b>	<b>0.05</b>	3.66
Hybrid-CL [6]	<b>0</b>	0.1	3.41
<b>Ours</b>	<b>0, <math>\sigma = 0</math></b>	<b>0.05</b>	<b>1.76</b>
<b>Ours FPR99</b>	<b>0, <math>\sigma = 0</math></b>	-	-

Table 3: Patch matching results evaluated on En *et al.* Benchmark [14] consisting of three multimodal datasets sampled on a uniform grid layout. The score is given in terms of FPR95. On the VeDAI dataset, we performed a stricter evaluation using FPR99 and reported the standard deviation out of 10 tests.

Our approach achieved a new SOTA performance when trained on the Liberty and Yosemite datasets, surpassing the previous SOTA by 24%. When trained on Notre Dame our approach is slightly outperformed by CS L2-Net [36] and Twin-Net [20]. We suspect it is due to the significant geometric deformations in Notre Dame, degrading the feature maps extracted by our Siamese CNN. Notre Dame also con-

Method	NOT	YOS	LIB	YOS	LIB	NOT	Mean
	LIB		NOT		YOS		
SIFT [24]	29.84		22.53		27.29		
MatchNet [40]	7.04	11.47	3.82	5.65	11.60	8.70	8.05
TL+AS+GOR [42]	1.95	5.40	4.80	5.15	6.45	2.38	4.36
L2-Net [36]	3.64	5.29	1.15	1.62	4.43	3.30	3.23
CS L2-Net [36]	2.55	4.24	0.87	1.39	3.81	2.84	2.61
L2-Net [36]	2.36	4.70	0.72	1.29	2.57	1.71	2.22
CS L2-Net [36]	1.71	3.87	0.56	1.09	2.07	1.30	1.76
Scale aware [22]	0.68	2.51	1.79	1.64	2.96	1.02	1.64
HardNet [26]	0.53	1.96	1.49	1.84	2.51	0.78	1.51
Twin-Net [20]	1.19	2.12	<b>0.41</b>	<b>0.69</b>	<b>1.58</b>	1.62	1.27
Exp-TLoss [38]	0.47	1.32	1.16	1.10	2.01	0.67	1.12
<b>Ours</b>	<b>0.35</b>	<b>0.91</b>	1.31	0.85	<b>1.58</b>	<b>0.41</b>	<b>0.9</b>

Table 4: Patch matching results evaluated on the UBC Benchmark [9]. Score is given in terms of FPR95. LIB: Liberty, NOT: Notredame, YOS: Yosemite.

sists of some extremely hard samples, that Twin-Net [20] might be able to mine better using its improved hard samples mining scheme.

#### 4.6. Attention maps

We further study the Transformer encoder self-attention mechanism by visualizing the attention weights as heatmaps. This allows to analyze the visual cues the encoder pays attention to. We show the attention heatmaps of four matching RGB and NIR pairs taken from the VIS-NIR Benchmark [3], originated from different scenes. The heatmaps are generated by upsampling the attention weights of the last encoder layer.

The resulting attention maps are presented in Fig. 3, showing the encoder learns to attend to modality-invariant feature locations, paying more attention to locations consisting of object blobs or their distinctive corners and edges. In the first pair 3a, the encoder summarizes the scene well by paying attention to both the bigger traffic sign in the middle and the second, smaller one in the background. In the second pair 3b, the encoder attends to the distinctively shaped tree on the left, as well as the house corner, which is a good modality-invariant feature. The third pair 3c contains two small houses and the encoder chooses to attend to both of them, also paying some attention to the grass fields in the foreground. In the fourth pair 3d, the encoder catches and attends the car in the middle of the scenes along with parts of the background house, but misses the black motor-bike in the NIR image, probably due to distinction difficulties originated from low pixel intensities.

#### 4.7. Ablation study

To better understand the contribution of each component in our proposal, we experiment with modifying one compo-

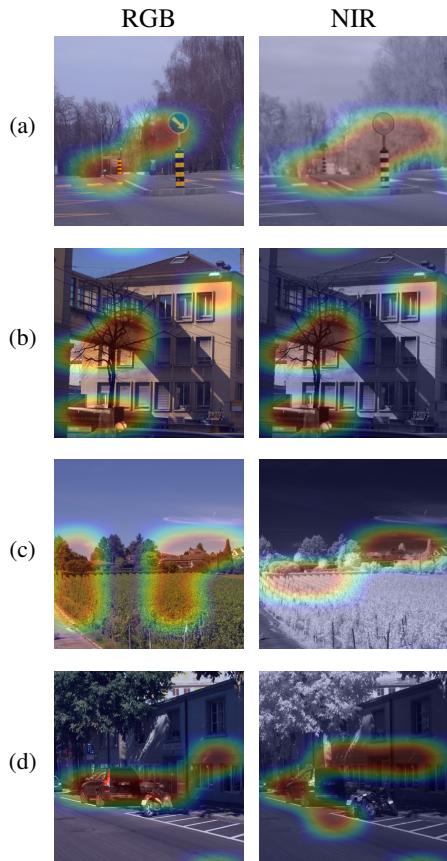


Figure 3: Attention heatmaps visualizing the Transformer encoder attention weights. The presented heatmaps show corresponding multimodal RGB and NIR images taken from various scenes of the VIS-NIR Benchmark [3].

CNN	Transformer	Attention		Residual	SPP	VIS-NIR
		Layers	Heads			
Siamese	-	-	-	-	+	1.77
Siamese	-	-	-	-	-	1.83
Siamese	Encoder	4	2	+	+	1.5
Siamese	Encoder	2	4	+	+	1.59
Siamese	Encoder+ Decoder	2	2	+	+	1.66
Pseudo Siamese	Encoder	2	2	+	+	2.03
Siamese	Encoder	2	2	-	+	DIV
<b>Siamese</b>	<b>Encoder</b>	<b>2</b>	<b>2</b>	<b>+</b>	<b>+</b>	<b>1.44</b>

Table 5: Ablation results evaluated on the VIS-NIR Benchmark [3]. Score is given in terms of FPR95. DIV means the model diverged and was not able to learn.

ment or related parameter at a time and measuring its impact. The experiments were performed on the VIS-NIR Benchmark [3], and are reported at Table 5. We first evaluate the impact of the Transformer encoder. By removing the Transformer and leaving the rest of the architecture intact, it is shown that adding the Transformer provides a 23% improvement. Removing also the SPP as well as the Transformer results in even a greater error. The performance is not improved by adding encoder layers or heads, nor adding a Transformer decoder on top of the encoder which degrades performance by 14%, probably due to overfitting. A CNN of non-shared weights, coined Pseudo-Siamese CNN and used in previous SOTA approaches [3, 6], ends up with inferior performance compared to the Siamese CNN, illustrating the importance of weight-sharing. An additional observation is the significance of the residual connection, as without it, the architecture cannot be trained end-to-end from scratch and the training diverges.

Dimensions	Type	VIS-NIR
-	-	1.63
1D	Fixed	1.54
	Learned	1.58
2D	Fixed	1.62
	Learned	<b>1.44</b>

Table 6: Positional encoding ablation results evaluated on the VIS-NIR Benchmark [3]. Score is given in terms of FPR95.

We also measure the impact of the different positional encoding formulation in Table 6, where we evaluated fixed and learned 1D and 2D positional encodings, following Parmar *et al.* [27] and Eq. 1. It follows that learning a 2D positional encoding yields the best performance, implying that

the encoder benefits from utilizing the original 2D spatial layout of the features.

The embedding dimension used by the network was studied in Table 7 by training the network from scratch using multiple dimensions. A larger embedding dimension can improve the network’s capacity, but can also lead to overfitting. The results in Table 7 show that  $\mathbb{R}^{128}$  is the ‘sweet spot’, as the model does not benefit from a larger descriptor size, and its performance is degraded by using a smaller descriptor.

Dimension	VIS-NIR
64	1.93
<b>128</b>	<b>1.44</b>
256	1.45

Table 7: Descriptor size ablation results evaluated on the VIS-NIR Benchmark [3]. The score is given in terms of the FPR95.

## 5. Conclusions

In this paper, we presented a novel approach for performing multimodal image patch matching using a Transformer encoder on top of Siamese CNN multiscale feature maps, utilizing long-range feature interactions as well as modality-invariant feature aggregations. We also introduced a residual connection shown to be essential for training Transformer-based networks from scratch. The proposed scheme achieves new SOTA performance when applied to contemporary multimodal patch matching benchmarks and the popular single modality UBC Benchmark, illustrating its generalizability.



## References

- [1] Cristhian Aguilera, Fernando Barrera, Felipe Lumbreras, Angel D. Sappa, and Ricardo Toledo. Multispectral image feature points. *Sensors*, 12(9):12661–12672, 2012. **1**
- [2] Cristhian Aguilera, Angel D. Sappa, and Ricardo Toledo. Lghd: A feature descriptor for matching across non-linear intensity variations. In *Image Processing (ICIP), 2015 IEEE International Conference on*, page 5. IEEE, Sep 2015. **5, 6**
- [3] C. A. Aguilera, F. J. Aguilera, A. D. Sappa, C. Aguilera, and R. Toledo. Learning cross-spectral similarity measures with deep convolutional neural networks. In *2016 IEEE Conference on Computer Vision and Pattern Recognition Workshops (CVPRW)*, pages 267–275, 2016. **2, 5, 6, 7, 8**
- [4] Cristhian A. Aguilera, Angel D. Sappa, Cristhian Aguilera, and Ricardo Toledo. Cross-spectral local descriptors via quadruplet network. *Sensors*, 17(4), 2017. **1, 2, 5, 6**
- [5] Vassileios Balntas, Edward Johns, Lilian Tang, and Krystian Mikolajczyk. Pn-net: Conjoined triple deep network for learning local image descriptors. *CoRR*, abs/1601.05030, 2016. **1, 2, 5, 6**
- [6] Elad Ben Baruch and Yosi Keller. Multimodal matching using a hybrid convolutional neural network. *CoRR*, abs/1810.12941, 2018. **1, 2, 3, 5, 6, 8**
- [7] Herbert Bay, Andreas Ess, Tinne Tuytelaars, and Luc Van Gool. Speeded-up robust features (surf). *Comput. Vis. Image Underst.*, 110(3):346–359, June 2008. **1**
- [8] Irwan Bello, Barret Zoph, Ashish Vaswani, Jonathon Shlens, and Quoc V. Le. Attention augmented convolutional networks. In *Proceedings of the IEEE/CVF International Conference on Computer Vision (ICCV)*, October 2019. **3**
- [9] M. Brown, G. Hua, and S. Winder. Discriminative learning of local image descriptors. *IEEE Transactions on Pattern Analysis and Machine Intelligence*, 33(1):43–57, 2011. **2, 5, 6, 7**
- [10] Nicolas Carion, Francisco Massa, Gabriel Synnaeve, Nicolas Usunier, Alexander Kirillov, and Sergey Zagoruyko. End-to-end object detection with transformers. In *Computer Vision – ECCV 2020*, pages 213–229, 2020. **3**
- [11] Jian Chen and Jie Tian. Real-time multi-modal rigid registration based on a novel symmetric-sift descriptor. *Progress in Natural Science*, 19:643–651, 05 2009. **1**
- [12] Jacob Devlin, Ming-Wei Chang, Kenton Lee, and Kristina Toutanova. BERT: Pre-training of deep bidirectional transformers for language understanding. In *Proceedings of the 2019 Conference of the North American Chapter of the Association for Computational Linguistics: Human Language Technologies, Volume 1 (Long and Short Papers)*, pages 4171–4186, Minneapolis, Minnesota, June 2019. Association for Computational Linguistics. **3, 4**
- [13] Alexey Dosovitskiy, Lucas Beyer, Alexander Kolesnikov, Dirk Weissenborn, Xiaohua Zhai, Thomas Unterthiner, Mostafa Dehghani, Matthias Minderer, Georg Heigold, Sylvain Gelly, Jakob Uszkoreit, and Neil Houlsby. An Image is Worth 16x16 Words: Transformers for Image Recognition at Scale. *arXiv e-prints*, page arXiv:2010.11929, Oct. 2020. **3**
- [14] S. En, A. Lechery, and F. Jurie. Ts-net: Combining modality specific and common features for multimodal patch matching. In *2018 25th IEEE International Conference on Image Processing (ICIP)*, pages 3024–3028, 2018. **1, 2, 3, 5, 6**
- [15] Aristides Gionis, Piotr Indyk, and Rajeev Motwani. Similarity search in high dimensions via hashing. In *Proceedings of the 25th International Conference on Very Large Data Bases, VLDB ’99*, page 518–529, San Francisco, CA, USA, 1999. Morgan Kaufmann Publishers Inc. **4**
- [16] Priya Goyal, Piotr Dollár, Ross B. Girshick, Pieter Noordhuis, Lukasz Wesolowski, Aapo Kyrola, Andrew Tulloch, Yangqing Jia, and Kaiming He. Accurate, large minibatch SGD: training imagenet in 1 hour. *CoRR*, abs/1706.02677, 2017. **5**
- [17] K. He, X. Zhang, S. Ren, and J. Sun. Spatial pyramid pooling in deep convolutional networks for visual recognition. *IEEE Transactions on Pattern Analysis and Machine Intelligence*, 37(9):1904–1916, 2015. **1, 3, 4**
- [18] Md. Tanvir Hossain, Guohua Lv, Shyh Wei Teng, Guojun Lu, and Martin Lackmann. Improved symmetric-sift for multi-modal image registration. In *Proceedings of the 2011 International Conference on Digital Image Computing: Techniques and Applications, DICTA ’11*, page 197–202, USA, 2011. IEEE Computer Society. **1**
- [19] M. Irani and P. Anandan. Robust multi-sensor image alignment. In *Sixth International Conference on Computer Vision (IEEE Cat. No.98CH36271)*, pages 959–966, 1998. **1**
- [20] Aman Irshad, Rehan Hafiz, Mohsen Ali, Muhammad Faisal, Yongju Cho, and Jeongil Seo. Twin-net descriptor: Twin negative mining with quad loss for patch-based matching. *IEEE Access*, 7:136062–136072, 2019. **2, 3, 6, 7**
- [21] M. Jahrer, Michael Grabner, and Horst Bischof. Learned local descriptors for recognition and matching. In *Proceedings of the Computer Vision Winter Workshop 2008*, pages 39–46. ., 2008. **1, 2**
- [22] Michel Keller, Zetao Chen, Fabiola Maffra, Patrik Schmuck, and Margarita Chli. Learning deep descriptors with scale-aware triplet networks. In *Proceedings of the IEEE Conference on Computer Vision and Pattern Recognition (CVPR)*, June 2018. **7**
- [23] Diederik P. Kingma and Jimmy Ba. Adam: A method for stochastic optimization. In Yoshua Bengio and Yann LeCun, editors, *3rd International Conference on Learning Representations, ICLR 2015, San Diego, CA, USA, May 7-9, 2015, Conference Track Proceedings*, 2015. **5**
- [24] David G. Lowe. Distinctive image features from scale-invariant keypoints. *Int. J. Comput. Vision*, 60(2):91–110, Nov. 2004. **1, 2, 5, 6, 7**
- [25] Rui Ma, Jian Chen, and Zhong Su. Mi-sift: Mirror and inversion invariant generalization for sift descriptor. In *Proceedings of the ACM International Conference on Image and Video Retrieval, CIVR ’10*, page 228–235, New York, NY, USA, 2010. Association for Computing Machinery. **5, 6**
- [26] A. Mishchuk, Dmytro Mishkin, Filip Radenović, and Jiri Matas. Working hard to know your neighbor’s margins: Local descriptor learning loss. In *NIPS*, 2017. **2, 3, 5, 6, 7**
- [27] Niki Parmar, Ashish Vaswani, Jakob Uszkoreit, Lukasz Kaiser, Noam Shazeer, Alexander Ku, and Dustin Tran. Im-

- age transformer. In Jennifer Dy and Andreas Krause, editors, *Proceedings of the 35th International Conference on Machine Learning*, volume 80 of *Proceedings of Machine Learning Research*, pages 4055–4064, Stockholm, Sweden, 10–15 Jul 2018. PMLR. [3](#), [8](#)
- [28] Adam Paszke, Sam Gross, Francisco Massa, Adam Lerer, James Bradbury, Gregory Chanan, Trevor Killeen, Zeming Lin, Natalia Gimelshein, Luca Antiga, Alban Desmaison, Andreas Kopf, Edward Yang, Zachary DeVito, Martin Raison, Alykhan Tejani, Sasank Chilamkurthy, Benoit Steiner, Lu Fang, Junjie Bai, and Soumith Chintala. Pytorch: An imperative style, high-performance deep learning library. In H. Wallach, H. Larochelle, A. Beygelzimer, F. d’Alché-Buc, E. Fox, and R. Garnett, editors, *Advances in Neural Information Processing Systems 32*, pages 8024–8035. Curran Associates, Inc., 2019. [5](#)
- [29] Dou Quan, Shuai Fang, Xuefeng Liang, Shuang Wang, and Licheng Jiao. Cross-spectral image patch matching by learning features of the spatially connected patches in a shared space. In C. V. Jawahar, Hongdong Li, Greg Mori, and Konrad Schindler, editors, *Computer Vision – ACCV 2018*, pages 115–130, Cham, 2019. Springer International Publishing. [5](#), [6](#)
- [30] Dou Quan, Xuefeng Liang, Shuang Wang, Shaowei Wei, Yanfeng Li, Ning Huyan, and Licheng Jiao. Afd-net: Aggregated feature difference learning for cross-spectral image patch matching. In *Proceedings of the IEEE/CVF International Conference on Computer Vision (ICCV)*, October 2019. [3](#)
- [31] Sebastien Razakarivony and Frederic Jurie. Vehicle detection in aerial imagery : A small target detection benchmark. *Journal of Visual Communication and Image Representation*, 34, 03 2015. [5](#)
- [32] Paul-Edouard Sarlin, Daniel DeTone, Tomasz Malisiewicz, and Andrew Rabinovich. Superglue: Learning feature matching with graph neural networks. In *Proceedings of the IEEE/CVF Conference on Computer Vision and Pattern Recognition (CVPR)*, June 2020. [3](#)
- [33] Florian Schroff, Dmitry Kalenichenko, and James Philbin. Facenet: A unified embedding for face recognition and clustering. In *Proceedings of the IEEE Conference on Computer Vision and Pattern Recognition (CVPR)*, June 2015. [3](#), [4](#)
- [34] Edgar Simo-Serra, Eduard Trulls, Luis Ferraz, Iasonas Kokkinos, Pascal Fua, and Francesc Moreno-Noguer. Discriminative learning of deep convolutional feature point descriptors. In *Proceedings of the IEEE International Conference on Computer Vision (ICCV)*, December 2015. [2](#), [3](#)
- [35] Aristeidis Sotiras, Christos Davatzikos, and Nikos Paragios. Deformable medical image registration: A survey. *IEEE transactions on medical imaging*, 32, 05 2013. [1](#)
- [36] Y. Tian, B. Fan, and F. Wu. L2-net: Deep learning of discriminative patch descriptor in euclidean space. In *2017 IEEE Conference on Computer Vision and Pattern Recognition (CVPR)*, pages 6128–6136, 2017. [2](#), [5](#), [6](#), [7](#)
- [37] Ashish Vaswani, Noam Shazeer, Niki Parmar, Jakob Uszkoreit, Llion Jones, Aidan N Gomez, Łukasz Kaiser, and Illia Polosukhin. Attention is all you need. In I. Guyon, U. V. Luxburg, S. Bengio, H. Wallach, R. Fergus, S. Vishwanathan, and R. Garnett, editors, *Advances in Neural Information Processing Systems*, volume 30. Curran Associates, Inc., 2017. [3](#)
- [38] Shuang Wang, Yanfeng Li, Xuefeng Liang, Dou Quan, Bowu Yang, Shaowei Wei, and Licheng Jiao. Better and faster: Exponential loss for image patch matching. In *Proceedings of the IEEE/CVF International Conference on Computer Vision (ICCV)*, October 2019. [1](#), [2](#), [5](#), [6](#), [7](#)
- [39] Xiaogang Wang and Xiaoou Tang. Face photo-sketch synthesis and recognition. *IEEE transactions on pattern analysis and machine intelligence*, 31:1955–67, 11 2009. [5](#)
- [40] Xufeng Han, T. Leung, Y. Jia, R. Sukthankar, and A. C. Berg. Matchnet: Unifying feature and metric learning for patch-based matching. In *2015 IEEE Conference on Computer Vision and Pattern Recognition (CVPR)*, pages 3279–3286, 2015. [1](#), [2](#), [7](#)
- [41] S. Zagoruyko and N. Komodakis. Learning to compare image patches via convolutional neural networks. In *2015 IEEE Conference on Computer Vision and Pattern Recognition (CVPR)*, pages 4353–4361, 2015. [1](#), [2](#), [5](#)
- [42] X. Zhang, F. X. Yu, S. Kumar, and S. Chang. Learning spread-out local feature descriptors. In *2017 IEEE International Conference on Computer Vision (ICCV)*, pages 4605–4613, 2017. [7](#)